

Si adatom binding and diffusion on the Si(100) surface: Comparison of *ab initio*, semiempirical and empirical potential results

A. P. Smith, J. K. Wiggs, and H. Jónsson

Department of Chemistry, BG-10, University of Washington, Seattle, Washington 98195

H. Yan

Department of Materials Science and Engineering, FB-10, University of Washington, Seattle, Washington 98195

L. R. Corrales

Molecular Science Research Center, Pacific Northwest Laboratory, Richland, Washington 99352

P. Nachtigall and K. D. Jordan

Department of Chemistry, University of Pittsburgh, Pittsburgh, Pennsylvania 15260

(Received 12 September 1994; accepted 4 October 1994)

The binding energies and configurations for single Si adatoms on the Si(100) surface are investigated theoretically. Detailed comparisons between previously published and new calculations using classical potentials, semiempirical formulations, and density functional theory (DFT) are made. The DFT calculations used both the plane-wave-pseudopotential approach in a periodic slab geometry and the Gaussian-orbital based all-electron approach employing cluster geometries. In the local-density approximation excellent agreement between the cluster and slab results was obtained. Inclusion of gradient corrections to the exchange-correlation energy significantly improves absolute binding energies and changes relative energies by as much as 0.3–0.5 eV depending on the particular exchange-correlation functional used. Binding energies and relative energies obtained using the classical potentials disagree with the gradient corrected DFT energies at about the 0.6–0.9 eV level, and most find qualitatively different local minima from those found in the DFT calculations. The semiempirical approaches give results intermediate in quality between those of the classical potentials and the *ab initio* calculations. Analysis of the energies and binding site geometries provides insight into the shortcomings of some of the classical potentials. © 1995 American Institute of Physics.

I. INTRODUCTION

Fundamental to progress in the accurate simulation of materials, particularly of nonequilibrium processes such as crystal growth, is the need for an accurate description of the interatomic interactions in a wide range of bonding environments. Not surprisingly theoretical modeling of bulk silicon and of processes on the silicon surface have attracted considerable attention. Many different classical interaction potentials (see Ref. 1) and a variety of semiempirical approaches² have been used in modeling silicon. In addition, *ab initio* calculations have been applied to silicon clusters,³ crystal structures,⁴ and surfaces.^{5,6}

The purpose of this paper is to test and compare these techniques on the problem of silicon adatom binding on the Si(100) surface. In this study we consider several classical potentials, including one specifically designed for the adatom binding problem,⁷ a recently developed semiempirical approach,⁸ and density functional theory in both the local and gradient-corrected density approaches, comparing calculations with slab and cluster geometries. For a few binding sites, quadratic configuration-interaction (QCI)⁹ calculations are also performed. We also compare with the results of previous calculations that have been performed on this system.^{7,10–17}

The reconstruction of the Si (100) surface has previously been systematically examined using both classical potentials and *ab initio* calculations, and most calculations agree on the essentials of the Si(100)2×1 reconstruction. The only sig-

nificant disagreement is that the *ab initio* calculations predict a tilt or buckling of the surface dimers,⁶ whereas the calculations with the classical potentials give a symmetrical structure. However, the *ab initio* calculations indicate that the energy lowering associated with buckling is small (about 0.035 eV/dimer). The ground state in the DFT calculations is actually an alternately buckled p(2×2) structure, although the uniformly buckled (2×1) structure is also a local minimum.

Isolated Si adatoms on the Si(100) surface have not been clearly seen in experiments, possibly because adatom diffusion is too fast. The previous theoretical calculations^{7,10–17} all predict anisotropic diffusion due to differing barriers in the directions parallel and perpendicular to the surface dimers. This has apparently been confirmed by experiments on island formation on the (100) surface,¹⁸ with the preferred diffusion direction being along the dimer rows in agreement with most of the calculations. The experimentally determined diffusion barrier is 0.67 ± 0.08 eV for diffusion parallel to the dimer rows. The barrier in the perpendicular direction was not determined directly, but the diffusion anisotropy of about 1000 at 550 degrees suggests a perpendicular barrier of about 1.0 eV.¹⁸

The adatom diffusion problem is clearly of relevance to understanding epitaxial growth of silicon. Our results, to be presented below, show that the most widely used classical potentials are seriously deficient in their description of the potential energy surface for the adatom, particularly for ada-

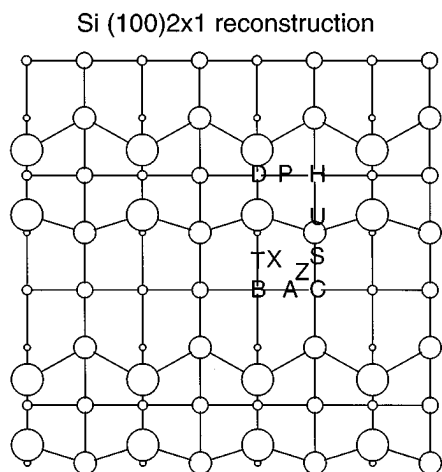


FIG. 1. Geometry of the (100) 2×1 reconstructed surface, showing the uniform asymmetric dimer reconstruction used in some of the LDA calculations. The labeled points mark out the “irreducible” region used to obtain the potential energy surface discussed in the text.

tom positions close to the epitaxial binding sites, where the model potentials overbind the adatom, and at the above-dimer epitaxial site they break the underlying dimer bond. In addition, the geometries obtained from the classical potentials are not even in qualitative agreement with the *ab initio* results.

On the other hand, qualitatively similar potential energy surfaces are obtained from the various *ab initio* calculations. There are, however, some quantitative differences between the results obtained from the local-density approximation (LDA) and the various nonlocal-density approximations (NLDA). Specifically, the adatom binding energies are lowered by 0.3 to 0.7 eV when using the PW91 functional,¹⁹ and by 1.1 to 1.8 eV when using the Becke3LYP functional.^{20,21} The relative energies of different surface structures are therefore changed by as much as 0.4–0.7 eV upon inclusion of nonlocal corrections in the density functional theoretical (DFT) calculations. Through extensive recent experience²² the Becke3LYP functional has proven to be a considerable improvement over LDA in matching experimental results for small molecules including atomization and harmonic vibrational energies, and has also apparently shown better agreement with experiment in some surface calculations.²³ Our results show that the PW91 results tend to recover part of the Becke3LYP correction, and therefore inclusion of either of these gradient corrections improves the quantitative description of Si binding on the Si(100) surface over that obtained with the LDA.

II. GEOMETRIES

The Si(100) 2×1 surface consists of rows of parallel Si dimers as shown in Fig. 1. The displacements of the surface atoms in forming dimers are in the direction of the surface projection of their dangling bonds, so that dimer formation satisfies half of the dangling bonds of the ideal Si(100) 1×1 surface. If buckling of the surface dimers is neglected, the irreducible set of potential adatom binding sites consists of

the quarter of the unit cell marked off by the labels in Fig. 1. We follow the notation of Srivastava and Garrison (SG)¹³ which is nearly the same as that used by Brocks, Kelly, and Car (BKC)¹¹ (the differences are the global minimum site which BKC label “M” and which we and SG label “S,” and the local minimum on the B–D line which BKC label “C” and which we and SG label “T”). We also add two additional local minima located in our LDA/slab calculations, “A” between “B” and “C,” and “P” between “D” and “H.” In addition to these local minima or potential local minima we have assigned labels to the other stationary points obtained in our DFT calculations, including the “Y” site which is the high point between “D” and “T,” and the “U,” “X,” and “Z” points which are saddle points between the “S” site and the “P,” “T,” and “A” sites respectively. The various sites are indicated in Fig. 1. The B and D sites are epitaxial—an adatom in one of these sites is in the correct (x,y) position for further growth of the Si diamond crystal structure—but we note here that the *ab initio* calculations do not find these positions to be even local minima for the isolated adatom on the surface, although the nearby “T” and “P” local minima might serve the same purpose.

After the reconstruction to form the dimers, each surface atom is left with one dangling bond. The classical potential models for the most part try to enforce tetrahedral geometries, and the different binding sites satisfy different numbers of these dangling bonds. On the other hand, except for the T site, all local minima found in the *ab initio* calculations correspond to structures in which the adatom is bound to two surface dangling bonds. In addition, the *ab initio* calculations reveal that the interactions of the adatom with Si atoms in the first and second sublayers are sizable, and many of the relaxed structures show a second or even third layer Si atom with five bonds, with the adatom then threefold coordinated.

III. METHODS

Although the ground state of an isolated Si atom has triplet spin multiplicity, for the strongly bound species considered here, it is expected that only the singlet states are important and all quantum mechanical calculations were carried out assuming a singlet state. Binding energies for each method are reported relative to the lowest energy reconstructed Si(100) 2×1 surface [i.e., a staggered $p(2\times 2)$ structure for the slab DFT calculations], plus a noninteracting triplet Si atom.

A. DFT calculations using slab models

In these calculations a slab-type geometry with periodic boundary conditions was employed. The surface unit cell consisted of eight layers of eight atoms each, with the lowest three layers frozen and with a 10 Å vacuum spacing between slabs. We considered atoms added to both the asymmetric (2×1) reconstructed surface and the staggered $p(2\times 2)$ surface, but the initial surface made little difference to the final adatom energy (less than 0.05 eV) except near the line from the C site to the H site (see Fig. 2). The electronic and ionic degrees of freedom were relaxed simultaneously using the Car–Parrinello approach.²⁴ Norm-conserving nonlocal pseudopotentials²⁵ were employed on the Si atoms to model

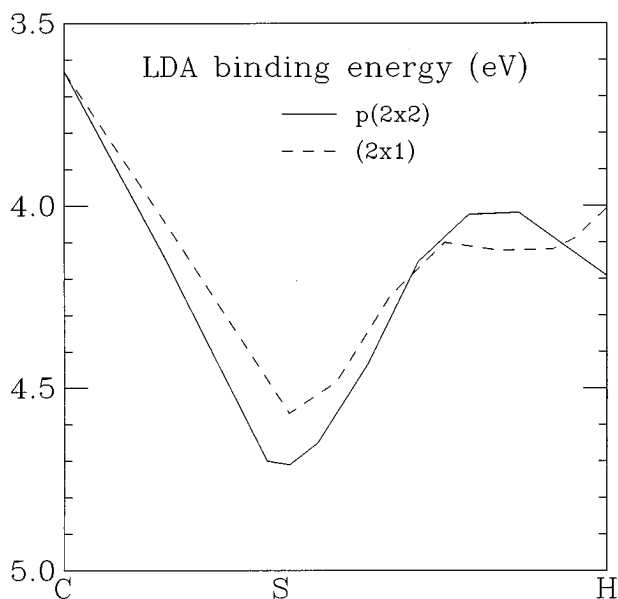


FIG. 2. Absolute binding energy for an adatom in the LDA-slab calculations along the C–H line for the 2×1 uniformly buckled and $p(2\times 2)$ alternating buckled surfaces, taken with reference to the corresponding ideal surface energies. The C–H line was the only part of the potential energy surface where this distinction was significant. There are actually two distinct S sites, with the $p(2\times 2)$ configuration being the true global minimum.

the core (i.e., 1s, 2s, and 2p) electrons and a plane wave basis set was employed. The geometry relaxations were done in the local density approximation (LDA), using the Perdew–Zunger parameterization of the Ceperley–Alder exchange correlation functional.²⁶ The gradient corrections^{19,21,27} to the total energies were calculated using the Perdew–Wang 1991 (PW91) formulation,¹⁹ which has been claimed to work well for surfaces,²⁸ and using the LDA geometries and charge densities. More details on the techniques used are given in Ref. 29. The technical differences between our calculations and two earlier plane-wave LDA calculations on the Si adatom problem are summarized in Table I.

As in previous calculations, the energy is calculated over an (x,y) grid, where x and y are parallel to the surface. At each (x,y) value the adatom is started from high above the surface and the distance from the surface (z) and the positions of the surface atoms are then optimized, subject to constraints discussed below. In some cases two different minima

TABLE I. Details of LDA slab model calculations.

	This work	MHO ^a	BK ^{c,b}
Atoms/layer	8	2	8
Layers (frozen)	8 (3)	6 (0)	12 (2)
Vacuum (Å)	10	14	9.5
Dimers	(2×1)	symm	$p(2\times 2)$
k points	1	1	4
Energy cutoff (Ry)	12	10	8
Pseudopotential	BHS ^c	Ihm-Cohen ^d	BHS ^c
Nonlocality	s, p	...	s, p

^aReference 10.

^cReference 30.

^bReference 11.

^dReference 25.

are found for a particular (x,y) value by using starting configurations with the adatom located closer to the surface as at the D site, or with a change in the positions of other atoms on the surface, as along the C–H line (see Fig. 2).

The Car–Parrinello code used in this study employs a modified steepest-descent dynamics for the ions. The fictitious mass and time step parameters used to balance electron and ion motion were optimized by means of a series of test runs for the Si surface. The rate of convergence varied from site to site, but typically near convergence the energy changes decreased by at least a factor of 2 every 100 time steps. Runs were halted when the energy decrease over 100 time steps was less than 0.01 eV. The forces on the atoms were also checked to ensure convergence.

A single converged geometry for the 65 atom slab system required roughly 1000 Car–Parrinello dynamics steps, using 50–80 CPU hours on an IBM RS6000/580 workstation. Most of the Car–Parrinello calculations were done using a parallel version of the code,³¹ running on Touchstone Delta and Intel Paragon systems. These calculations required about 9 hours using 64 nodes of the Touchstone Delta or 300 node-hours per configuration on the Intel Paragon. Nearly 100 different geometries were optimized.

B. DFT and QCISD(T) calculations with cluster models

We have also calculated Si adatom binding energies on the Si(100)- 2×1 surface using the LDA, NLDA, and QCISD(T)⁹ methods, together with Gaussian-type basis sets and cluster models. The cluster model LDA calculations made use of the exchange functional of Dirac³² and the correlation functional of Vosko, Wilk, and Nusair³³ (this combination of functionals will be referred to as VWN). The corresponding NLDA calculations made use of the Becke3LYP functional (which is comprised of the three parameter nonlocal exchange functional of Becke²⁰ and the nonlocal correlation functional of Lee, Yang, and Parr²¹) as well as the BP86 functional (which is comprised of the exchange and correlation functionals of Becke²⁷ and Perdew,³⁴ respectively). Previous studies of the interactions of hydrogen with the Si(100)- 2×1 surface^{35–37} have shown that the Becke3LYP functional gives results in excellent agreement with those from QCISD(T) calculations.³⁷ [The QCISD(T) procedure generally yields reaction energies correct to 0.2 eV.]

In the DFT calculations a $\text{Si}_{15}\text{H}_{16}$ cluster was used to model the clean Si(100) 2×1 surface and a $\text{Si}_{16}\text{H}_{16}$ cluster [depicted in Fig. 3(b)] was used to model a Si adatom at the S, D, D*, T, H, and P sites. Additional calculations using the DFT method as well as the QCISD(T) method were carried out using Si_9H_{12} and $\text{Si}_{10}\text{H}_{12}$ clusters [depicted in Fig. 3(a)] to model the clean surface and the D and D* adsorption sites, respectively. The hydrogen atoms were introduced to saturate the subsurface Si atoms.

The initial geometries of the clusters, in the absence of the Si adatom, were obtained using a procedure described previously.³⁶ The top two (three) silicon layers were allowed to relax during geometry optimization of the Si_9H_{12} and $\text{Si}_{10}\text{H}_{12}$ ($\text{Si}_{15}\text{H}_{16}$ and $\text{Si}_{16}\text{H}_{16}$) clusters, while the rest of the

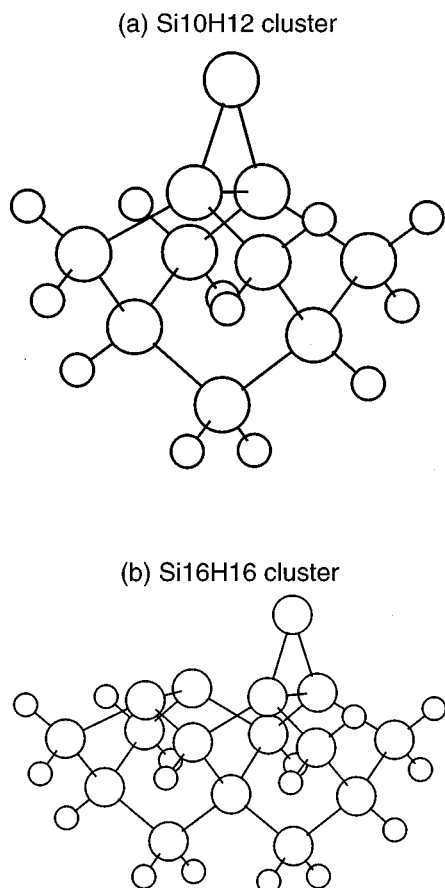


FIG. 3. Geometries of the (a) Si₁₀H₁₂ and (b) Si₁₆H₁₆ clusters used in the cluster calculations (for the D site). The large spheres represent Si atoms and the small spheres the H atoms, and in both cases the adatom is at the top of the figure, with a surface dimer directly underneath.

Si atoms and cluster-terminating H atoms were kept frozen. The geometries of the Si₁₅H₁₆ and Si₁₆H₁₆ clusters were optimized using both the VWN and Becke3LYP functionals, whereas the geometries of the Si₉H₁₂ and Si₁₀H₁₂ clusters were optimized using only the Becke3LYP functional. The geometry optimizations were carried out using analytical gradients, an effective-core potential³⁸ on the silicon atoms to model the Si 1*s*, 2*s*, and 2*p* orbitals, a valence double-zeta-plus-polarization (EC-DZP) function basis set on the Si atoms, and a double-zeta (DZ) basis set on the H atoms.³⁹ (In the geometry optimizations of the Si₁₅H₁₆ and Si₁₆H₁₆ clusters, the d functions were not included on the five Si atoms in the lowest two layers.)

At the optimized geometries single-point all-electron calculations were performed using the Becke3LYP, BP86, and VWN functionals together with the 6-31G* basis set.⁴⁰ The QCISD(T) calculations on the Si₉H₁₂ and Si₁₀H₁₂ clusters used the geometries optimized with the Becke3LYP functional. [The procedure for carrying out the QCISD(T) calculations is described in Ref. 36.] The cluster model calculations were carried out using the GAUSSIAN 92 program suite.⁴¹

In the absence of symmetry and using the Becke3LYP functional, a single cycle in the geometry optimization of the

Si₁₆H₁₆ cluster took about 4 CPU hours and a complete optimization typically required 40 CPU hours on an IBM RS6000/375 workstation. Thus the geometry optimizations of the cluster models using the GAUSSIAN 92 DFT code required the same order of magnitude computational effort as did the optimizations of the slab models using the Car-Parrinello molecular dynamics approach.

C. A semiempirical approach

The semiempirical approach used in this work is similar to the extended Hückel method first used by Corrales and Rossky to simulate liquid and amorphous sulfur.⁸ For large systems this approach scales linearly in the number of atoms, as do the calculations with classical potentials. A detailed description of the parametrization for silicon and the modifications of this approach for use in optimizations is presented elsewhere.⁴² The most important modification is that for a fixed nuclear configuration the electronic wave function is determined by direct minimization methods rather than by a Monte Carlo simulated annealing method, as was used in Ref. 8.

The variables in this method, aside from the atomic positions, are the hybridization state of the atoms (a combination of the *sp*, *sp*², and *sp*³ hybrid orbitals) and the orientations of the associated orbitals. The energies of the hybridized orbitals are determined from their fractional *s* and *p* character, with a penalty being associated with a dangling bond designed to give the correct energy for the *s*²*p*² atomic ground state. The hybridizations and orientations are varied to optimize the overlaps *S*_{*ij*} between neighboring atoms, and then these are used to form bonds using a 2×2 (or 4×4, if π -bonding is included) one-electron extended Hückel Hamiltonian. Using this localized molecular orbital approximation, the binding energy is pairwise additive and is calculated using the lowest energy molecular orbital eigenvalues for each bonding pair. An empirical pairwise additive core repulsion term is also included, from a fit to gas phase Si₂ spectroscopic data. The final energy includes a long range nonbonding interaction in the form of a modified Buckingham potential.

The model has the flexibility of excluding or including π bonding interactions. The former will be referred to as the free dangling bond (FDB) approximation in which π overlaps are ignored. The inclusion of π bonding interactions leads to shorter bond lengths for both the dimer bond and the backbonds to the surface, and can lead to tilted dimers whereas only symmetric dimers are obtained in the FDB approach.

In the calculations presented here the surface was modeled with a slab (periodic boundary conditions) with 16 atoms per layer and 12 layers, plus the adatom. This approach can also be used with clusters with no change or additional approximation required. In fact it is not even necessary to cap the dangling bonds with hydrogen atoms, although this can be done if needed.

These calculations for a 192 atom slab system were converged using a Newton-Raphson method for the FDB approach, and a zero velocity Verlet algorithm when π bonds

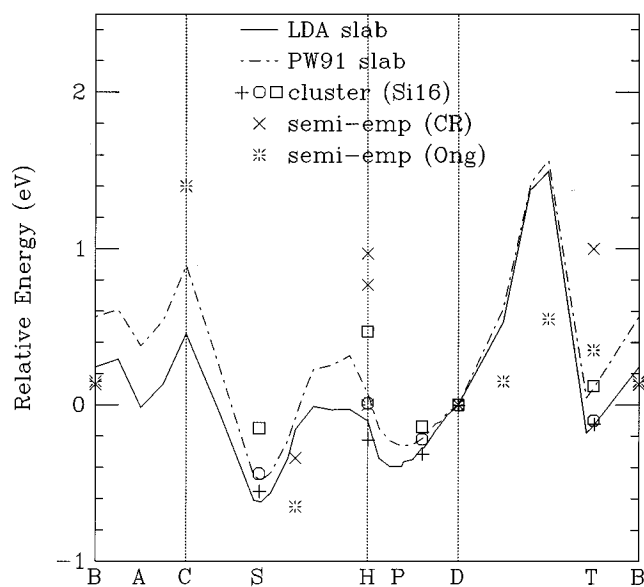


FIG. 4. Relative energies along the boundary curve for the different *ab initio* and semiempirical techniques, taking the D site energy to be zero. The slab model calculations in the LDA and with the PW91 gradient corrections are designated by solid and dashed lines, respectively. The open symbols denote results obtained from the cluster model DFT calculations: the + signs are with LDA exchange-correlation, the circles with BP and the squares with B3LYP nonlocal exchange-correlation. The crosses and asterisks represent the Corrales-Rosky and Ong semiempirical results respectively. The cluster results include the relaxation corrections discussed in the text.

were included. The former required 2–3 hours and the latter 3–4 hours of CPU time on an HP 730 workstation, and so were at least an order of magnitude faster than both the cluster and slab DFT calculations, and can address significantly larger systems.

D. Classical potentials

Due to the tremendous interest in the simulation of the properties of silicon, considerable effort has been put into developing empirical interatomic potentials. More than a dozen classical potentials for silicon have appeared in the literature during the past decade, and more are being developed. Recent reviews have compared some of these potentials in terms of their performance in describing the energetics and properties of bulk and surface structures.^{1,43}

Following Carlsson's terminology,⁴⁴ most of these interatomic potentials can be classified as either cluster potentials, such as the Stillinger-Weber potential,⁴⁵ or cluster functionals, as exemplified by the Tersoff potential.⁴⁶ The cluster potentials describe bonding in terms of explicit two-body and three-body interactions. In the Stillinger-Weber potential the angular dependence of the three-body interaction is designed to penalize deviations from tetrahedral angles in the structure. The Tersoff potential,⁴⁶ is based on the idea that bond order depends on local coordination around the bonded pair, not simply on relative positions of triplets of atoms. The atomic interaction energy is represented by pairwise functions of the interatomic distances, r_{ij} , modulated by a function that depends explicitly on the bond angles θ_{ijk} .

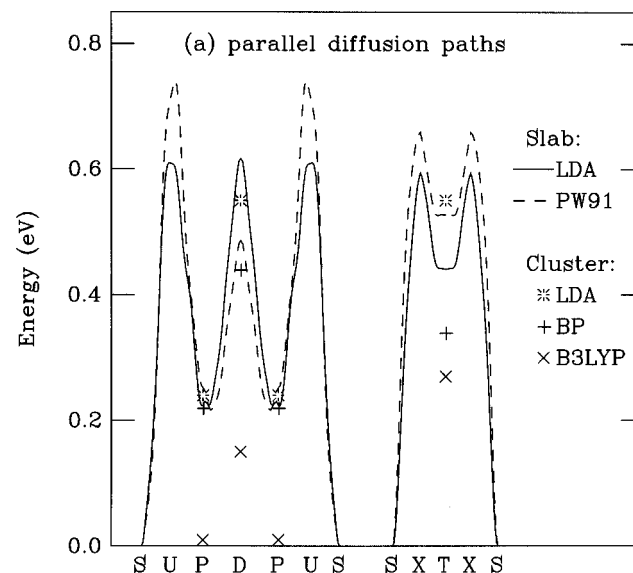
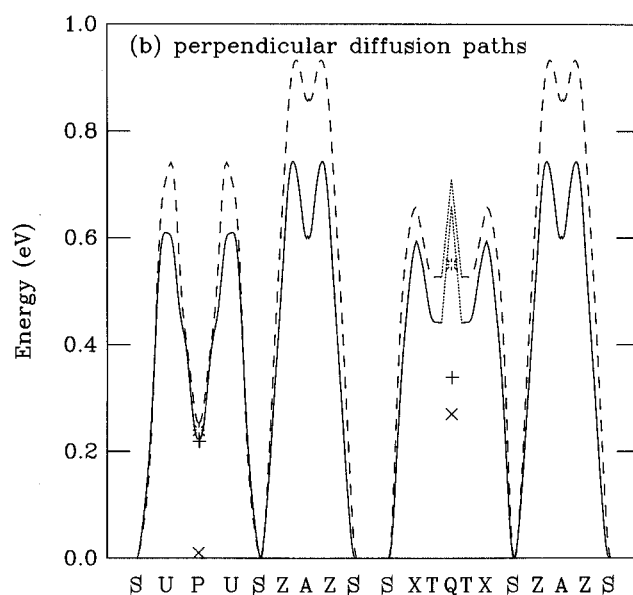
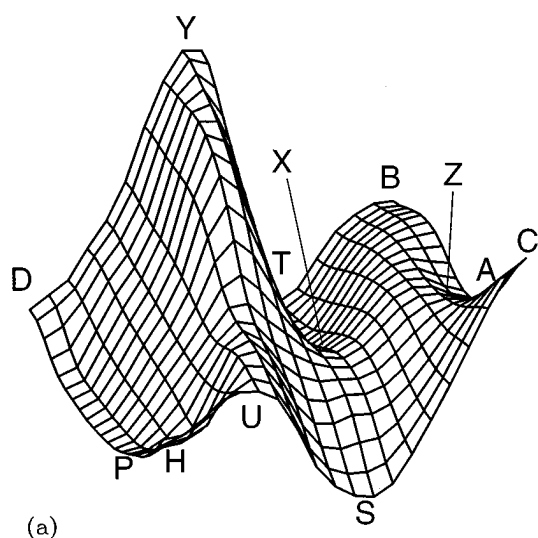
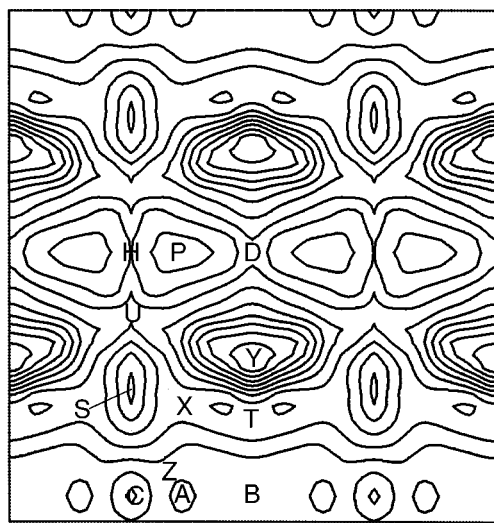


FIG. 5. Energies along the possible diffusion paths (a) parallel and (b) perpendicular to the dimer rows, relative to the global minimum energy at the S site. The lines were generated with the same spline fits used in Fig. 6 to the slab model calculations and the points calculated with the cluster model are represented by symbols. For both parallel and perpendicular diffusion there are two possible paths—in the perpendicular case the second path utilizes an exchange process T-Q-T drawn with dotted lines. Note that in the cluster calculations the T and Q sites coincide so there is no barrier to exchange.

Bolding and Andersen⁴⁷ have generalized the Tersoff potential to take into account π bonding effects. In their potential form, the attractive term is expressed as a sum of σ - and π -bonding terms with different proportions. The fitting data base is large, with an emphasis on small clusters and high pressure solid phases. The fact that the Bolding-Andersen potential explicitly includes π -bonding may have contributed to its success in modeling the Si(111)2 \times 1 surface.¹ As we find below, its relative success on the Si(100)2 \times 1 surface



(a)



(b)

FIG. 6. (a) A 3D plot and (b) a contour plot of the potential energy surface obtained from the PW91 gradient-corrected slab calculations. The surface was generated by a Fourier spline fit to all 52 grid-point energies as a sum of 158 sinusoidal functions with the symmetry of the dimer reconstructed surface. The fitted energy surface passes through all the calculated points and is otherwise designed to be as smooth as possible.

suggests π -bonding is an important characteristic of Si surface configurations in general.

The Stillinger–Weber and Tersoff potentials, and their variants,^{7,48,49} have been widely used in simulations of Si(100) surface properties^{12–16,7} and in studies of the energetics of adsorption sites, diffusion paths, and energy barriers on the Si(100) 2×1 surface. A few studies of the diffusion of Si adatoms on stepped surfaces and of dimer formation and mobility have also been carried out.^{15,16} However, the reliability of these empirical potentials for describing such surface processes has yet to be established.

IV. RESULTS AND DISCUSSION

Figures 4–7 depict the potential energy surface obtained from our calculations and from some of the earlier

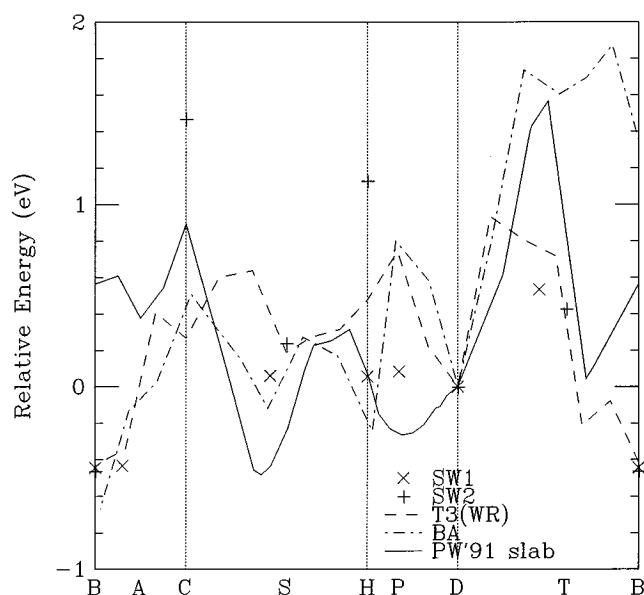


FIG. 7. Relative energies obtained for the classical potentials and the PW91 slab model calculations following the boundary around the irreducible region, taking the zero of energy at the D site for the classical potentials and at the P site (the nearest local minimum) for the PW91 calculations. SW1 and SW2 indicate the results obtained from two different Stillinger–Weber potentials (see Refs. 12 and 14); W–R and B–A designate results obtained using the Wang–Rockett (or T3) and Bolding–Andersen (BA) potentials, respectively.

calculations.^{12,14,17} Two of the figures (Figs. 4 and 7) depict relative values of the potential energy surface along the path B–C–H–D–B. The results from the slab calculations with PW91 exchange correlation are shown in all the figures for reference purposes. Figures 5(a) and 5(b) depict the possible diffusion paths, and Figs. 6(a) and 6(b) show the PW91 energy surface in more detail. Tables II–IV list the binding energies and selected key geometrical parameters at the local minima and other sites of interest. Additional information on the geometries is provided in Tables V–VIII. Figure 8 shows the structures obtained from the slab model calculations, relaxed in the LDA.

The most detailed characterization of the potential energy surface for the interaction of a Si adatom on the Si(100) surface was obtained using the LDA/slab approach, and these results will be discussed first, even though they are not necessarily the most reliable. The results of the LDA calculations using the slab and cluster models are described in Secs. IV A and IV B, respectively. The results of DFT calculations using nonlocal density functionals and of the QCI calculations are summarized in Sec. IV C. The semiempirical results are presented in Sec. IV D. Finally, the results obtained with the classical potentials are discussed in Sec. IV E.

A. LDA/slab model

There have been two prior plane-wave based LDA calculations of the energetics of a Si adatom on the Si(100) surface. Some details of these calculations are given in Table I. The first, by Miyazaki and co-workers¹⁰ used a very small

TABLE II. Adatom binding energy E_b (eV), height above the ideal surface z (Å), and bond-length of nearest surface dimer l (Å) obtained from density functional and CR semi-empirical calculations. All cluster model results except those designated by LDA* include corrections for surface relaxation, as described in the text. Note that D* and T are identical sites (with adatom and dimer atom switched) for the slab and cluster DFT calculations, but they are distinct sites in the classical potential and semiempirical calculations.

		Slab		Cluster ^c				CR ^e	
		LDA ^a	PW91 ^b	LDA opt. geometry			NLDA opt. geometry		
				LDA* ^d	LDA ^d	BP86	Becke3LYP	Becke3LYP	
B	E_b	3.85	3.25					3.37	
	z	-0.69						1.40	
	l	2.36						2.52	
A	E_b	4.11	3.44						
	z	-0.67							
	l	2.38							
C	E_b	3.63	2.92					0.11	
	z	-1.07						1.25	
	l	2.30						2.63	
S	E_b	4.71	4.30	4.84	5.04	4.17	3.53	3.57	3.84
	z	0.72			0.87			0.87	1.70
	l	2.36			2.45			2.47	2.44
H	E_b	4.19	3.74	4.61	4.71	3.72	2.94	2.95	2.73
	z	1.33			1.33			1.40	1.74
	l	2.30			2.48			2.52	2.42
P	E_b	4.49	4.08	4.71	4.80	3.95	3.51	3.56	
	z	1.51			1.57			1.66	
	l	2.55			2.63			2.72	
D	E_b	4.09	3.81	4.45	4.49	3.73	3.47	3.42	3.50
	z	1.97			1.95			1.93	2.12
	l	2.39			2.39			2.40	2.34
D*	E_b	4.22	3.71	4.49	4.61	3.83	3.33	3.30	3.36
	z	-0.21			0.20			0.36	1.46
	l	4.48			4.48			4.45	3.89
T	E_b	4.22	3.71	4.49	4.61	3.83	3.33	3.30	2.50
	z	-0.45			0.27			0.21	2.20
	l	2.37			2.24			2.23	2.42

^aPresent LDA/slab calculations.

^bSlab calculations with Perdew-Wang '91 gradient correction.

^cAll cluster binding energies other than those in the LDA* column include the relaxation corrections discussed in the text.

^dCluster calculations using the VWN local density approximation.

^eSemiempirical calculations using Corrales-Rosky technique.

surface with only two atoms per layer, and thus only one dimer in the surface unit cell. For this cell the single adatom represents a 50% coverage of the surface. Their results differ considerably from those obtained using larger cells (Ref. 11 and the present work), although there are some qualitative similarities that can be drawn. Most of the differences are attributable to the small surface unit cell which distorted the preferred relaxations of the Si dimer rows.

The other calculation, performed by Brocks, Kelly, and Car (BKC),¹¹ used a unit cell consisting of twelve layers of eight atoms each. Brocks *et al.* reported the S site (M in their notation) to be the global minimum, the H, T (their C), and B sites to be local minima, and the D site to be a transition state. They also concluded that Si adatom diffusion is anisotropic with activation energies of 0.6 and 1.0 eV for diffusion

TABLE III. Adatom binding energy E_b (eV) at the D and D* sites calculated using the QCISD(T) and DFT methods and the Si_9H_{12} and $\text{Si}_{10}\text{H}_{12}$ cluster models.

Method	Binding energies (eV)	
	D	D*
QCISD(T) ^a	3.08	2.81
Becke3LYP ^b	3.34	2.99
BLYP ^c	3.27	3.09
BP86 ^d	3.58	3.33
LDA ^e	4.33	4.04

^aQuadratic CI method (Ref. 9).

^dSee Refs. 27 and 34.

^bSee Refs. 21 and 20.

^cSee Refs. 32 and 33.

^eSee Refs. 27 and 21.

TABLE IV. Adatom binding energy E_b (eV), height above the ideal surface z (Å), and dimer bond-length l (Å) for various classical potentials.

		SW1 ^a	SW2 ^b	T1 ^c	T2 ^d	T3 ^e	BA ^f
B	E_b	3.14	3.16	3.43	3.51	3.55	2.21
	z	1.13	1.31	1.25	1.22	1.37	1.09
	l		2.69	2.53	2.51	2.47	2.53
C	E_b		1.23	2.37	2.31	2.87	3.05
	z		0.92	0.51	0.61	0.78	0.53
	l		2.54	2.35	2.34	2.37	2.31
S	E_b	2.64	2.46	2.99	3.08	2.95	3.68
	z	1.70	1.92	1.69	1.67	1.93	1.05
	l		2.48	2.38	2.39	2.39	2.42
H	E_b	2.64	1.57	2.46	2.68	2.66	3.80
	z	1.51	1.88	1.46	1.47	1.49	0.91
	l		2.61	2.58	2.58	2.48	2.48
D	E_b	2.70	2.70	3.26	3.27	3.14	3.56
	z	1.36	1.54	1.63	1.63	1.66	1.21
	l		3.80	3.65	3.40	3.67	3.71
T	E_b	2.16	2.27	2.57	2.47	2.27	1.96
	z	2.04	2.27	2.31	2.30	2.31	2.16
	l		2.47	2.39	2.39	2.38	2.43

^aFrom Ref. 12, calculated using the Stillinger–Weber potential (Ref. 45).^bFrom Ref. 14, calculated using a modified version of the Stillinger–Weber potential (Ref. 49).^cFrom Ref. 13, calculated using the version of the Tersoff potential described in Ref. 46.^dCalculated using the version of the Tersoff potential given in Ref. 48.^eCalculated using the Wang–Rockett potential (Ref. 7).^fCalculated using the Bolding–Anderson potential (Ref. 47).

along and perpendicular to the surface dimer row, respectively, in good agreement with the subsequent experimental observations.¹⁸

Our LDA slab calculations give relative energies of the S, B, D, and T sites and of the saddle point between S and T (designated here as X) in qualitative agreement with those of Brocks *et al.* We also find the details of the geometries at the

TABLE V. Relaxed geometry at the S site according to different computational methods [see Fig. 8(a)].

Method	Bond lengths (Å)				
	A–D ₁	A–D ₂	A–B ₁	D ₁ –D' ₁	D ₁ –B ₁
LDA ^a	2.35	2.34	2.38	2.36	2.39
B3LYP ^b	2.40	2.40	2.41	2.51	2.43
C-R	2.46	2.47	3.14	2.44	2.33
W-R	2.47	2.47	3.33	2.39	2.43
B-A	2.42	2.42	2.43	2.42	2.45
Method	Bond angles (deg)				
	D ₁ –A–D ₂	D ₁ –A–B ₁	A–D ₁ –D' ₁	A–D ₁ –B ₁	D' _{1/2} –D _{1/2} –B ₁
LDA ^a	97	61	125	60	94/119
B3LYP ^b	99	61	125	60	104
C-R	87	47	103	82	105
W-R	88	47	108	86	103
B-A	104	61	117	60	107

^aCalculated using the slab model.^bCalculated using the cluster model.

TABLE VI. Relaxed geometry at the local minimum closest to the unbroken dimer site (either the P site or the D site depending on the computational method) [see Fig. 8(b)].

Method	Bond lengths (Å)			
	A–D ₁	A–D' ₁	D ₁ –D' ₁	D ₁ –B ₁
LDA ^a (P)	2.28	2.32	2.55	2.32
B3LYP ^b (P)	2.33	2.33	2.73	2.36
C-R (D)	2.42	2.42	2.34	2.35
B-A (D)	2.40	2.40	2.48	2.39
Method	Bond angles (deg)			
	D ₁ –A–D' ₁	A–D ₁ –B ₁	A–D ₁ –D' ₁	
LDA ^a (P)	67	89	57	
B3LYP ^b (P)	72	105	54	
C-R (D)	58	122	61	
B-A (D)	62	125	59	

^aCalculated using the slab model.^bCalculated using the cluster model.

S and T minima to agree with those reported by Brocks *et al.* However, since we used a finer grid (0.38×0.77 Å initially, with additional points added in “interesting” regions) to explore the irreducible region, we were able to discern some details apparently missed by these authors. In particular, we find a local minimum P between the H and D sites and a local minimum A between the B and C sites. We also find that the B and H sites are first-order saddle points rather than minima as reported by Brocks *et al.* The binding energies from these calculations are summarized in the first column of Table II. In this table we also include results for the D* site, the structure of which (in the *ab initio* treatments) is identical to that of the T site [see Fig. 8(c)], but which is accessed through a dimer-breaking process at the D site rather than *via* the S–T path.

As may be seen from Fig. 8, several of the low-energy

TABLE VII. Relaxed geometry at the broken dimer D site [see Fig. 8(c)].

Method	Bond lengths (Å)				
	A–D ₁	A–D' ₁	A–B ₁	D ₁ –D' ₁	D ₁ –B ₁
LDA ^a	2.19	2.31	2.59	4.48	2.52
B3LYP ^b	2.23	2.23	3.20	4.43	2.45
C-R	2.43	2.43	3.84	3.89	2.34
W-R	2.31	2.31	3.85	3.67	2.32
B-A	2.24	2.24	3.74	3.71	2.36
Method	Bond angles (deg)				
	D ₁ –A–D' ₁	D ₁ –A–B ₁	A–D ₁ –B ₁	B ₁ –A–B ₂	B ₁ –D ₁ –B ₂
LDA ^a	169	63	66	94	97
B3LYP ^b	170	50	86	74	103
C-R	106	36	106	60	110
W-R	105	88	113	58	108
B-A	112	37	109	62	109

^aCalculated using the slab model.^bCalculated using the cluster model.

TABLE VIII. Relaxed geometry at the B site according to different computational methods [see Fig. 8(c)].

Method	Bond lengths (Å)			
	A-D ₁	A-D ₂	D ₁ -D ₁ '	D ₁ -B ₁
LDA ^a	2.35	2.58	2.39	2.40
C-R	2.55	2.55	2.52	2.31
W-R	2.39	2.39	2.47	2.34
B-A (1)	2.50	2.50	2.53	2.37
B-A (2)	2.68	2.68	2.47	2.41

Method	Bond angles (deg)			
	D ₁ -A-D ₂	A-D ₁ -D ₁ '	A-D ₂ -D ₂ '	A-D ₁ -B ₁
LDA ^a	178	177	165	72
C-R	116	143	143	103
W-R	123	155	155	103
B-A (1)	125	149	149	99
B-A (2)	134	157	157	66

^aCalculated using the slab model.

configurations contain 3-membered rings of bonded atoms, with near-60° bond angles (see Tables V–VIII). These configurations also often involve fivefold coordination of a subsurface atom.

As noted above, Brocks *et al.* considered the path S–D–S for diffusion along the dimer rows and the path S–B–S for diffusion perpendicular to the dimer rows, obtaining from LDA calculations barrier heights of 0.6 and 1.0 eV, respectively. Our LDA calculations give a barrier of 0.63 eV, close to that of Brocks *et al.*, for the S–D–S path, although the barrier we find is at the U position—the full path is S–U[†]–P–D[†]–P–U[†]–S [see Fig. 1 and Fig. 5(a)], where the “†” denotes a first order saddle point. We also find that the alternative path, S–X[†]–T–X[†]–S, has a barrier of 0.54 eV, which is slightly lower than that for the S–D–S path, in contradiction to the results of Brocks *et al.* The energy difference of 0.09 eV between the two paths is less than possible inaccuracies in these calculations however and so the disagreement may not be significant. The lowest energy paths for perpendicular diffusion have an overall barrier height of 0.71 eV, determined by the Z[†] saddle point. The full path for perpendicular diffusion requires crossing the H–D line, and we find two such paths: S–Z[†]–A–Z[†]–S–U[†]–P–U[†]–S and S–Z[†]–A–Z[†]–S–X[†]–T–Q[†]–T–X[†]–S where Q[†] is the symmetric transition state (0.66 eV) for interconversion of two asymmetric T=D* sites, and so this second path actually involves an exchange process with two atoms in a surface dimer. These calculations thus indicate that ac-

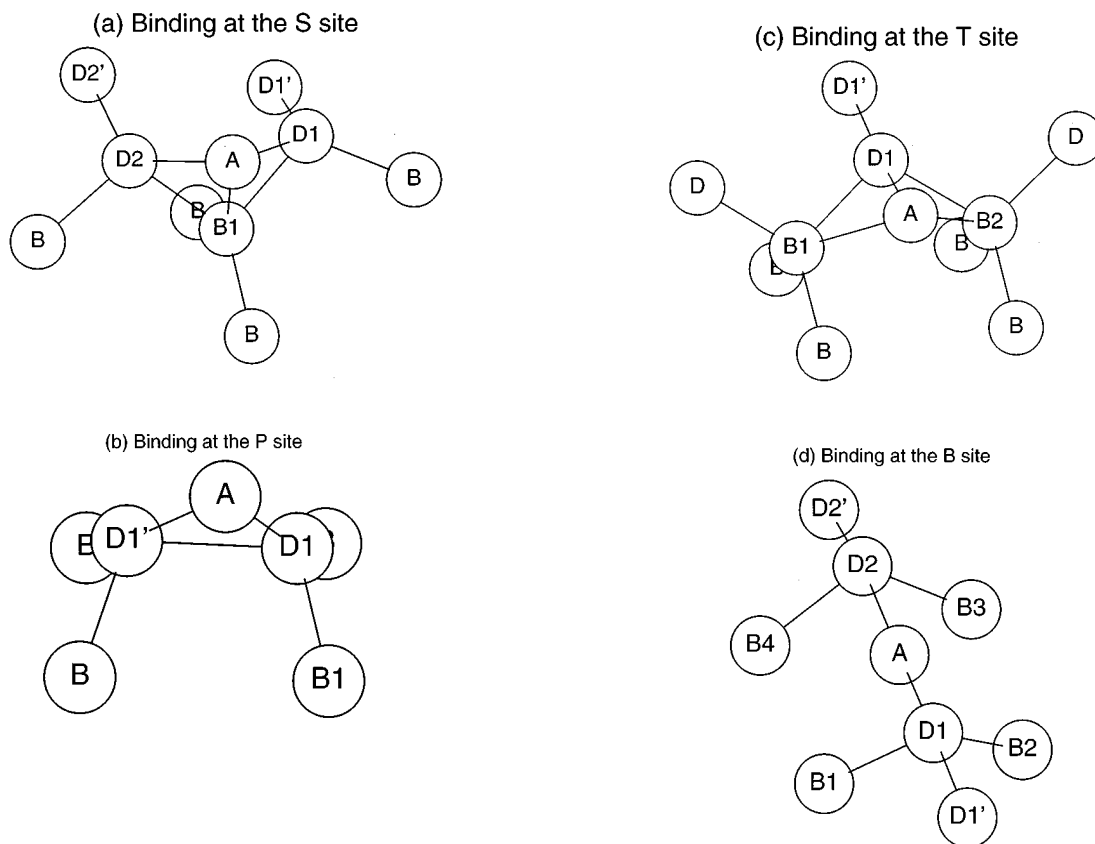


FIG. 8. Geometries of some local minima and saddle-point sites from the LDA slab calculations, with the labeled angles and bond distances listed in Tables V–VIII. The adatom and surface dimer atoms are designated as “A” and “D,” respectively. Subsurface atoms are denoted by “B.” These are (a) the S site, (b) the P site, (c) the T (or broken dimer D) site, and (d) the B site. In the broken dimer site, atoms A and D₁ are switched relative to the T site. Lines are drawn to signify bonds between atoms separated by less than 2.7 Å.

According to the LDA, Si adatom diffusion is nearly isotropic, having activation energies of 0.54–0.63 eV for diffusion in the parallel direction, and 0.71 eV in the perpendicular direction. In Sec. IV C it is shown that upon the inclusion of nonlocal exchange correlation corrections the calculations predict a stronger anisotropy in the adatom diffusion, more consistent with the experimental results¹⁸ (see also Fig. 5).

B. Cluster models

Before discussing the LDA results obtained using the cluster models, we first consider the problem of the adequacy of cluster models for describing geometrical relaxation. If the errors due to incomplete treatment of relaxation are different at different sites, this will cause errors in the relative energies of these sites. We are not aware of any prior systematic study addressing this problem.

There are basically two approaches that can be taken to estimating the errors associated with the use of the cluster models. One is to repeat the cluster calculations with much larger clusters. This would be a very computationally expensive undertaking. The alternative approach, and that adopted here, is to repeat the slab model calculations, but with the geometrical relaxation being constrained approximately as in the cluster models. Such constrained slab model optimizations were carried out on the D, H, P, T, and S sites. In these calculations the positions of most of the Si atoms are kept frozen in their positions optimized for the clean Si(100)2×1 surface; only those Si atoms, that are allowed to relax in Si₁₆H₁₆ cluster model, are allowed to relax in the constraint slab model calculations. The differences between the Si adatom binding energies obtained from the constrained and unconstrained slab model calculations provide estimates of the neglected relaxation energy in the cluster model.

These calculations show that due to incomplete treatment of geometry relaxation, the cluster model LDA calculations underestimate the binding energies at the D, P, H, T, and S sites by 0.04, 0.09, 0.10, 0.12, and 0.20 eV, respectively. The same procedure, but with the relaxation corrections estimated using the PW91 exchange-correlation functional gave cluster relaxation corrections of 0.05, 0.08, 0.10, 0.15, and 0.14 eV for the same sites. These results indicate that the Si₁₆H₁₆ cluster model gives a better description of some sites (D, P, and H for example) than of others (T and S), and that the errors in the relative energies introduced by incomplete treatment of geometrical relaxation are as large as 0.16 eV (or 0.11 eV in the NLDA case). For the calculation of potential energy surfaces for use in studies of the dynamics, it is desirable to reduce the errors in the relative energies to 0.1 eV or less. Our calculations therefore show that the cluster models employed here are almost large enough to meet this criterion, but larger cluster models are desirable. In spite of this shortcoming, moderate size cluster models are especially valuable because they can be used to carry out QCI or other calculations that would not be feasible for the slab models.

Table II reports Si adatom binding energies obtained from the various DFT calculations and from the CR semi-empirical calculations. All cluster results, except those labeled LDA*, include the relaxation corrections discussed

above, with the NLDA results using the corrections estimated from the PW91/slab calculations. In the ensuing discussion cluster results will include the relaxation corrections, unless stated otherwise.

The LDA/slab binding energies are, on average, 0.36 eV lower than the LDA/cluster energies. This discrepancy can be attributed to the use of different basis sets in the two sets of calculations and to the use of pseudopotentials in the slab model calculations. However, the relative energies of individual adsorption sites for the slab and cluster models in the LDA are in excellent agreement (see Fig. 4).

C. NLDA and QCI calculations

The inclusion of gradient corrections lowers the binding energy significantly, as can be seen from Table II. The changes are 0.3–0.7 eV in the slab model when using the PW91 functional, and 0.8–1.0 and 1.1–1.8 eV in the cluster model when using the BP86 and Becke3LYP functionals, respectively. These results indicate that the inclusion of gradient corrections in density functional theory is needed to improve the binding energies, and also has a significant effect on the relative energies between different points on the potential energy surface.

In order to evaluate the various correlation functionals, we have calculated the binding energies for the D and D* sites at both the QCISD(T) and DFT levels of theory and using a Si₁₀H₁₂ model. The results of these calculations are summarized in Table III. As found in earlier studies,³⁷ the DFT calculations with the Becke3LYP functional give the best agreement with the QCISD(T) binding energies. Using the QCISD(T) results as the best estimates of the true binding energies, we conclude that the LDA calculations overestimate the binding energies by up to 1.2 eV. The calculations with the BLYP functional (comprised of the exchange functional of Becke²⁷ and the LYP correlation functional) give binding energies within 0.1 eV of the Becke3LYP values, whereas calculations with the BP86 and PW91 functionals give binding energies 0.2–0.3 eV larger. The D/D* energy difference is nearly the same for all (both local and nonlocal) DFT calculations as well as for the QCISD(T) calculations. However, from examination of Table II, it is seen that the inclusion of nonlocal corrections to the LDA energies is important for some of the other energy differences. Comparison of the results of the various DFT calculations leads to the conclusion that it is the choice of the nonlocal correlation functional rather than the choice of the nonlocal exchange functional that is primarily responsible for the differences between the PW91 and Becke3LYP results.

The inclusion of the PW91 gradient corrections to the energies leads to significant changes in the diffusion barriers, although the paths remain unchanged. In the PW91 slab model the lowest energy path for diffusion along the surface dimer row is again the S–T–S path with barrier at X[‡] of 0.60 eV (see Fig. 6). The barrier at Z[‡] is increased to 0.91 eV and the barrier at U[‡] is increased to 0.71 eV. The Z[‡] barrier is again the highest barrier in the low energy pathways for diffusion in the perpendicular direction in the PW91 slab calculations. The anisotropy is then 0.31 eV, as opposed to 0.17

eV found in the LDA calculations, very close to the experimental value of 0.33 eV.

The cluster calculations were carried out only for some of the stationary points and only addressed diffusion along the dimer rows. The relative energies obtained with the BP86 functional agree with the PW91/slab results to within 0.1 eV except at the T site. The differences between the cluster and slab results at the T site are attributable to differences in the bonding geometries—in the cluster calculations the central atom at this T/D* site had only the two surface bonds, while in the slab calculations the corresponding atom was bonded to two underlying atoms also [see Fig. 8(c) and the A–B₁ distance in Table VII]. Since the cluster T site was already symmetric, there is no need for a Q site barrier between opposite T sites, and the cluster results are shown at the Q site position in Fig. 5.

Use of the Becke3LYP functional, however, significantly reduces the relative energy differences between the S site and the P and T local minima, and also the D site barrier, suggesting that the associated barriers are also significantly lower. In fact a parallel diffusion barrier as low as 0.15 eV is not excluded by the Becke3LYP results (see Fig. 5).

A three-dimensional plot and contour plot of the potential energy surface for the PW91 gradient-corrected slab calculations is given in Fig. 6. This figure also demonstrates that diffusion in the T–S channel to the side of the dimer rows, rather than over the top of the dimer via the D site, is preferred.

Based on these NLDA results we believe that the diffusion on the Si(100)2×1 surface is anisotropic with a diffusion barrier of 0.4–0.6 eV for diffusion along the surface dimer rows, and about 0.9 eV for perpendicular diffusion.

D. Semiempirical calculations

Both sets of semiempirical calculations predict the S site to be the global minimum and correctly obtain other qualitative features of the energy landscape. Quantitatively, the CR calculations in the FDB approximation give S–D[†] and S–D* energy differences in fair agreement with the PW91/slab model results. This is quite different from the results of all the empirical potential calculations discussed below. However, the CR–FDB semiempirical calculations find the B site to be too low and the T, H, and C sites to be too high in energy (relative to the S site, and comparing with the PW91/slab model results), and produce incorrect geometries for the S and T sites (see Table II) with the adatom sitting much too high above the surface. Also, in the CR calculations the D* and T sites are inequivalent with the latter lying about 0.9 eV higher in energy. The CR–FDB calculations also found two distinct local minima at the H site separated by 0.2 eV, depending on which of the neighboring atoms the adatom binds to, and this may be related to signs of similar multivalued behavior in the energetics of the *ab initio* calculations.

The inclusion of π bonds in the CR method allows other geometries and coordinations, partly because the equilibrium dimer position is closer to the surface. For example, the S site has a local minimum similar to that found with the FDB approximation, with the adatom high above the surface.

However, with π bonding included there is a second local minimum with the adatom much closer to the surface and bonded to a second layer atom, although in this model high coordinations are excluded and this second layer atom is then forced to break a bond with an atom in the third layer. This modified S site adatom configuration leads to a geometry similar to the DFT calculations, although the energy is higher than that of the other S site local minimum.

Previously published results based on the semiempirical tight-binding CNDO technique¹⁷ are also shown in Fig. 4 and correspond somewhat more closely to the *ab initio* calculations—in particular finding a higher B–S energy difference and lower energies at the H and T sites than do the CR results. However, the CNDO calculations again give a geometry for the S site with the adatom too high above the surface. In addition the CNDO calculations found only the broken dimer D* site with apparently no barrier to dimer breaking.

When compared to the classical potential results reviewed below, the semiempirical calculations make qualitative improvements in describing the potential energy surface for the adatom, but do not seem to significantly improve the geometric description of most of the binding sites. A possible cause for this problem in both sets of calculations is the neglect of slightly higher coordination environments for the Si atoms, which may require the use of d-orbitals. Higher coordination is also possible by including π bonding interactions between three distinct atoms. In general, the inclusion of π bonds between a pair of atoms remains pairwise additive; inclusion of 3-orbital interactions between three atoms would represent a higher order calculation. An added difficulty in the CR approach is the need for additional off-diagonal parameters in the modified Hückel matrices.

E. Classical potentials

Figure 7 shows the relative energies for the various classical potential models, with the PW91 slab results shown for reference. The path is again around the region given in Fig. 1. Table IV lists the binding energies and vertical heights of the adatom on the labeled sites above the ideal 2×1 surface.

Both the Stillinger–Weber and Tersoff potentials (with modifications) produce qualitatively similar descriptions of the adatom potential energy surface. Both sets of potentials find the global minimum at the epitaxial B site, and find that the underlying dimer bond is readily broken with another local minimum at the other epitaxial (D) site. Using the Stillinger–Weber potential (SW1 in the table and figures), Zhang *et al.*¹² identified local minima at B, near-B, S, H, near-H, D, and T sites, but not at the C site—all these local minima are depicted in Fig. 7. With a modified SW potential⁴⁹ (SW2), Toh and Ong¹⁴ obtained qualitatively similar results, except at the H site, which they found to be a saddle point separating two adjacent D sites, and without the near-B and near-H sites. Their local minima and the C and H saddle point energies are also given in the figures. The calculations using the Tersoff potential and its modified versions^{13,7} give energy differences similar to those obtained with the Stillinger–Weber potential, although the C site is found to be a local minimum rather than a saddle point.

The potential energy surfaces obtained with the Stillinger–Weber and Tersoff potentials are quite different from those found in the *ab initio* calculations. The global minimum and some of the local minima determined with the classical potentials are in fact not local minima but saddle points in the *ab initio* calculations. This seems to be mostly attributable to overbinding of the epitaxial sites by the classical potentials, which are designed to prefer tetrahedral bonding geometries. At the B site, which the Stillinger–Weber and Tersoff potentials find as a global minimum but the *ab initio* results find to be about 1 eV above the minimum, the classical potentials also allow too great a relaxation of the neighboring dimers towards the adatom.

In general the classical potentials give quite different geometries for the local minima than those obtained from the *ab initio* calculations. The most striking difference in geometry is at the epitaxial site directly above a surface dimer, where all the classical potentials (except the Bolding–Andersen potential, discussed separately below) predict the dimer bond to break with no (or an extremely low) barrier, so that the D site consists of the adatom bonded to the underlying dimer atoms which are no longer bonded to each other. The *ab initio* calculations, in contrast, find a barrier of at least 0.8 eV to the breaking of the dimer bond by direct insertion of the adatom, and give a broken-dimer (D^*) structure very different from that obtained by the classical methods (see Table VII). In the *ab initio* calculations the adatom is able to bond to the fully bonded dimer, although it prefers to be at a low-symmetry position (the P site) while doing this, and does open the dimer bond slightly (see Table VI).

The classical potentials, again aside from the Bolding–Andersen potential, also share with the semiempirical approaches a failure to describe the S site geometry correctly [see Fig. 8(a) and Table V]. The T site as described by the classical potentials is also very different from that of the *ab initio* calculations. The classical potentials, not surprisingly, put the adatom at an angle about 109° from the dimer to which it bonds, while the *ab initio* calculations place it almost at the same height above the surface as the dimer atoms (i.e., a 180° angle), and bonded to several underlying atoms, in a configuration that is identical to the broken dimer D^* site, but with two of the atoms switched.

Previous reviews¹ of the classical potentials have suggested that it may be impossible to construct a totally global or transferable potential, but it seems clear that the current potentials have several artifacts that must be corrected, in particular the penalization of bond angles below 90 degrees found to be the cause of errors in modeling small Si clusters.¹

The Bolding–Andersen potential gives a somewhat different picture of the Si adatom interactions. In particular, an adatom approaching a dimer does not spontaneously break the dimer bond—the energy barrier to bond breaking is about 1 eV. On the other hand, close to the B site, in the direction of the C site, the adatom sinks below the surface and bonds with numerous subsurface atoms, while a local minimum at the B site above the surface (similar to that found with the other classical potentials) has the adatom bonded to the surface dimer atoms, and has a much higher energy. For this

second B site the energy is in relatively good agreement with the *ab initio* results (see right-hand side of Fig. 7). Excluding the unphysical B site, the H site is the lowest energy site for the B–A potential, which may be due to an excessive π -bonding contribution. In addition the B–A potential does a somewhat better job describing the binding geometries, particularly at the S site (see Table V).

Thus the B–A potential seems to do well for geometries with up to five well-distributed bonds on an atom, or up to three bonds on one side of the atom, where the effective coordination is reasonably low. However, at the H site with 4 bonds on one side of the adatom, or at the unphysical B site with 6 or more bonds on the adatom, the B–A potential obtains an energy that is far too low. A “very high coordination” penalty to exclude the unphysical B site and raise the energy at the H site should significantly improve its behavior.

V. CONCLUSIONS

We have considered a wide variety of techniques for the interaction of a silicon adatom with the $\text{Si}(100)2\times 1$ surface. In the density functional calculations, gradient corrections proved to be important for the relative energies of the various stationary points on the potential energy surface, causing changes of up to 0.7 eV. In the local density approximation, the relative energies calculated in the slab and cluster models agree to within 0.1 eV. There are additional differences of up to 0.2 eV for some surface binding sites due to insufficient relaxation of the geometries with the cluster models used. The slab calculations with PW91 gradient corrections give barriers of 0.60 and 0.91 eV for parallel and perpendicular adatom diffusion, respectively, both in good agreement with the experimental estimates.¹⁸ The low energy pathways (see Fig. 5) are found to be $S-X^\ddagger-T-X^\ddagger-S$ for parallel diffusion and either $S-U^\ddagger-P-U^\ddagger-S-Z^\ddagger-A-Z^\ddagger-S$ or $S-X^\ddagger-T-Q^\ddagger-T-X^\ddagger-S-Z^\ddagger-A-Z^\ddagger-S$ for perpendicular diffusion, where the second perpendicular diffusion path involves an exchange process with one of the surface dimers. The cluster calculations were unfortunately not able to directly address the diffusion barriers, but the effects on the binding site energies suggested that with B3LYP exchange-correlation the parallel diffusion barrier could be considerably lower than 0.6 eV. The LDA slab calculations find the same diffusion paths as the PW91 slab calculations, but with lower barriers and less anisotropy, and so indicate that the NLDA is needed to obtain an anisotropy as large as that observed experimentally.

Comparison with existing classical interaction potentials demonstrated that they are inadequate for describing the energetics and the geometrical arrangements of the binding sites of a silicon adatom on the $\text{Si}(100)2\times 1$ surface. There appear to be two fundamental areas of discrepancy between the standard classical and *ab initio* results. First, the classical potentials overbind the epitaxial B site, and second, they fail to find the three-membered rings and fivefold coordinated atoms that are important in several of the *ab initio* structures. The geometries are improved with the Bolding–Andersen potential, but even this potential does not provide a good qualitative description of the energetics. The semiempirical calculations give qualitatively better energies, but also fail to

give highly coordinated bonding geometries. It may be possible to modify the Bolding–Andersen potential (by inclusion of a larger penalty for overcoordination) and the semi-empirical methods (by inclusion of d orbitals) to obtain better agreement with the *ab initio* results.

Our conclusion that existing classical potentials do poorly in describing the interaction of a Si adatom with the Si(100) surface is disturbing because of the great deal of effort that has already gone into classical simulations of growth processes on the Si surface. It is possible that the deficiencies of the classical potentials are less significant for the later stages of growth when the adatoms have started to cluster and most atoms have relatively high coordination environments. Otherwise full *ab initio* quantum mechanical treatments may be essential to reliably describe the crystal growth of silicon.

Note added in proof. After these calculations were complete we discovered that the VWN functional used in the cluster DFT calculations actually used parameters fitted to the random phase approximation (RPA) rather than to the Ceperley–Alder data (both parametrizations are given in Ref. 33). Our more recent calculations find that this changes the relative energy differences for Si structures by no more than 0.05 eV, and is therefore unlikely to have any significant effect on the results in this work.

ACKNOWLEDGMENTS

H.Y. and H.J. were supported by the Department of Energy under Award No. DE-FG06-91ER14224. A.P.S. and J.K.W. were supported by the National Science Foundation under Award No. CHE-9217294 (CARM). L.R.C. was supported by the Division of Chemical Sciences, Office of Basic Energy Sciences, U.S. Department of Energy under Contract No. DE-AC06-76RLO 1830 with Battelle Memorial Institute, which operates the Pacific Northwest Laboratory. K.D.J. acknowledges support from the National Science Foundation under Grant No. CHE9121306. We would like to thank Dr. Barry Bolding of Cray Research for providing the code with the Bolding–Andersen potential. Computer time was made available on the Delta by PNL–Battelle in Richland, WA, and on a Paragon supercomputer by the San Diego Supercomputer Center.

¹H. Balamane, T. Halicioglu, and W. A. Tiller, *Phys. Rev. B* **46**, 2250 (1992).

²A. H. Harker and F. P. Larkins, *J. Phys. C: Solid State Phys.* **12**, 2497 (1979); L. Goodwin, A. J. Skinner, and D. G. Pettifor, *Europhys. Lett.* **9**, 701 (1989).

³K. Raghavachari, *J. Chem. Phys.* **84**, 5672 (1986), and references therein.

⁴M. T. Yin and M. L. Cohen, *Phys. Rev. B* **26**, 5668 (1982); M.T. Yin, *ibid.* **30**, 1773 (1984); M. T. Yin and M. L. Cohen, *ibid.* **29**, 6996 (1984); R. J. Needs and R. M. Martin, *ibid.* **30**, 5390 (1984); R. Biswas, R. M. Martin, R. J. Needs, and O. H. Nielsen, *ibid.* **30**, 3210 (1984); K. J. Chang and M. L. Cohen, *ibid.* **30**, 5376 (1984); **31**, 7819 (1985).

⁵M. T. Yin and M. L. Cohen, *Phys. Rev. B* **24**, 2303 (1981).

⁶K. C. Pandey, in *Proceedings of the 17th International Conference on the Physics of Semiconductors*, San Francisco, CA, 1984, edited by D. J. Chadi and W. A. Harrison (Springer, New York, 1985); M. C. Payne, N. Roberts, R. J. Needs, M. Needels, and J. D. Joannopoulos, *Surf. Sci.*

211/212, 1 (1989); N. Roberts and R. J. Needs, *ibid.* **236**, 112 (1990); S. Ihara, S. L. Ho, T. Uda, and M. Hirao, *Phys. Rev. Lett.* **65**, 1909 (1990); Inder P. Batra, *Phys. Rev. B* **41**, 5048 (1990).

⁷J. Wang and A. Rockett, *Phys. Rev. B* **43**, 12571 (1991).

⁸L. R. Corrales and P. J. Rossky, *Chem. Phys. Lett.* **194**, 363 (1992).

⁹J. A. Pople, M. Head-Gordon, and K. Raghavachari, *J. Chem. Phys.* **87**, 5968 (1987).

¹⁰T. Miyazaki, H. Hiramoto, and M. Okazaki, *Jpn. J. Appl. Phys.* **29**, L1165 (1990).

¹¹G. Brocks, P. J. Kelly, and R. Car, *Phys. Rev. Lett.* **66**, 1729 (1991).

¹²Z. Zhang, Y. Lu, and H. Metiu, *Surf. Sci.* **248**, L250 (1991).

¹³D. Srivastava and B. J. Garrison, *J. Chem. Phys.* **95**, 6885 (1991).

¹⁴C. P. Toh and C. K. Ong, *Phys. Rev. B* **45**, 11120 (1992).

¹⁵C. Roland and G. H. Gilmer, *Phys. Rev. B* **46**, 13 428, 13 437 (1992).

¹⁶Z.-H. Huang and R. E. Allen, *J. Vac. Sci. Technol. A* **9**, 876 (1991).

¹⁷C. K. Ong, *J. Phys. Chem. Solids* **54**, 183 (1993).

¹⁸Y.-W. Mo and M. G. Lagally, *Surf. Sci.* **248**, 313 (1991); Y.-W. Mo, J. Kleiner, M. B. Webb, and M. G. Lagally, *Phys. Rev. Lett.* **66**, 1998 (1991).

¹⁹J. P. Perdew, in *Electronic Structure of Solids '91*, edited by P. Ziesche and H. Eschrig (Akademie, Berlin, 1991); J. P. Perdew and Y. Wang (unpublished).

²⁰A. D. Becke, *J. Chem. Phys.* **98**, 5648 (1993).

²¹C. Lee, W. Yang, and R. G. Parr, *Phys. Rev. B* **37**, 785 (1988).

²²B. G. Johnson, P. M. W. Gill, and J. A. Pople, *J. Chem. Phys.* **98**, 5612 (1993); K. Kim and K. D. Jordan, *J. Phys. Chem.* (in press).

²³P. Nachtigall, K. D. Jordan, and C. Sosa, *J. Chem. Phys.* (in press).

²⁴R. Car and M. Parrinello, *Phys. Rev. Lett.* **55**, 2471 (1985).

²⁵G. B. Bachelet, D. R. Hamann, and M. Schluter, *Phys. Rev. B* **26**, 4199 (1982).

²⁶J. P. Perdew and A. Zunger, *Phys. Rev. B* **23**, 5048 (1981).

²⁷A. D. Becke, *Phys. Rev. A* **33**, 3098 (1988).

²⁸J. P. Perdew *et al.*, *Phys. Rev. B* **46**, 6671 (1992).

²⁹M. C. Payne, M. P. Teter, D. C. Allen, T. A. Arias, and J. D. Joannopoulos, *Rev. Mod. Phys.* **64**, 1045 (1992).

³⁰J. Ihm and M. L. Cohen, *Solid State Commun.* **29**, 711 (1979).

³¹J. K. Wigg and H. Jonsson, *Comp. Phys. Comm.* **81**, 1 (1994).

³²P. A. M. Dirac, *Proc. Cam. Phil. Soc.* **26**, 376 (1930).

³³S. H. Vosko, L. Wilk, and M. Nusair, *Can. J. Phys.* **58**, 1200 (1980).

³⁴J. P. Perdew, *Phys. Rev. B* **33**, 8822 (1986).

³⁵P. Nachtigall, K. C. Janda, and K. D. Jordan, *J. Chem. Phys.* **95**, 8652 (1991).

³⁶P. Nachtigall, C. Sosa, and K. D. Jordan, *J. Phys. Chem.* **97**, 11666 (1993).

³⁷P. Nachtigall, C. Sosa, and K. D. Jordan, *J. Chem. Phys.* (in press).

³⁸W. R. Wadt and P. J. Hay, *J. Chem. Phys.* **82**, 284 (1985).

³⁹The effective core pseudopotential given in Ref. 38 together with the LP-31G valence basis set (built into GAUSSIAN 92), augmented by a set of polarization functions with exponent $\alpha=0.45$ was used for Si atoms, and the double-zeta basis set from T. H. Dunning and P. J. Hay, *Modern Theoretical Chemistry* (Plenum, New York, 1976) was used for H atoms.

⁴⁰W. J. Hehre, R. Ditchfield, and J. A. Pople, *J. Chem. Phys.* **56**, 2257 (1972); P. C. Hariharan and J. A. Pople, *Theor. Chim. Acta* **28**, 213 (1973); M. S. Gordon, *Chem. Phys. Lett.* **76**, 163 (1980); T. Clark, J. Chandrasekhar, G. W. Spitznagel, and P. v. R. Schleyer, *J. Comp. Chem.* **4**, 294 (1983).

⁴¹M. J. Frisch, G. W. Trucks, H. B. Schlegel, P. M. W. Gill, B. G. Johnson, M. W. Wong, J. B. Foresman, M. A. Robb, M. Head-Gordon, E. S. Replogle, R. Gomperts, J. L. Andres, K. Raghavachari, J. S. Binkley, C. Gonzalez, R. L. Martin, D. J. Fox, D. J. Defrees, J. Baker, J. J. P. Stewart, and J. A. Pople, GAUSSIAN 92/DFT, Gaussian, Inc., Pittsburgh, PA, 1992.

⁴²L. R. Corrales (unpublished).

⁴³S. J. Cook and P. Clancy, *Phys. Rev. B* **47**, 7686 (1993).

⁴⁴A. E. Carlsson, in *Solid State Physics: Advances in Research and Applications*, edited by H. Ehrenreich and D. Turnbull (Academic, New York, 1990), Vol. 43.

⁴⁵F. H. Stillinger and T. A. Weber, *Phys. Rev. B* **31**, 5662 (1985).

⁴⁶J. Tersoff, *Phys. Rev. B* **37**, 6991 (1988).

⁴⁷B. C. Bolding and H. C. Andersen, *Phys. Rev. B* **41**, 10568 (1990).

⁴⁸J. Tersoff, *Phys. Rev. B* **38**, 9902 (1988).

⁴⁹J. P. van der Eerden, G. Z. Liu, F. de Jong, and M. J. Anders, *J. Cryst. Growth* **99**, 106 (1990).